POLITECNICO
MILANO 1863

Dani Gabriele

Spacecraft Attitude Dynamics

Earth Pointing of 6U Spacecraft

May 13, 2021

Contents

1 Introduction

The aim of this project is to simulate the complete attitude dynamics of a 6U spacecraft that perform a low earth orbit.
The simulation will account the presence of the principal disturbance torques along with the actual performance of the selected ADCS components.
A preliminary estimation of mass properties has been carried out, based on the model in figure 1.

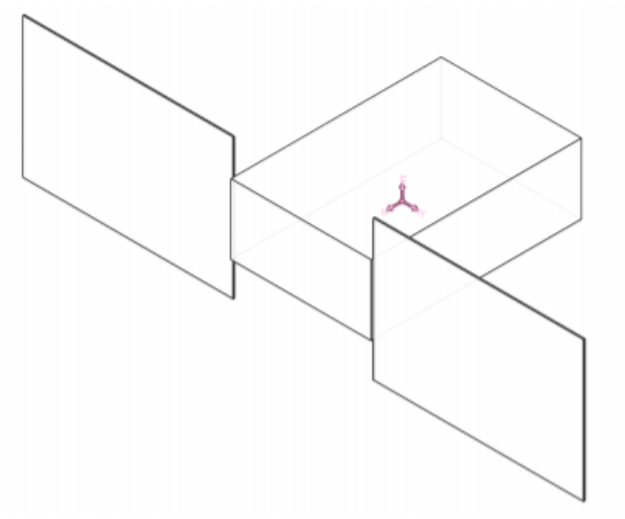

Figure 1: *Model of the 6U cubesat*

Table 1: *Mass and size of the S/C*

	Mass [kg]	**Size** [m]
Main body	9.0	$0.3 \times 0.2 \times 0.1$
Solar panels (single panel)	0.6	0.3×0.2

$$J = \begin{bmatrix} 0.09 & 0 & 0 \\ 0 & 0.14 & 0 \\ 0 & 0 & 0.07 \end{bmatrix} \text{ kg} \cdot \text{m}^2$$

$$x_{\text{CG}} = \begin{bmatrix} 0.01 & 0 & 0 \end{bmatrix}^{\intercal} \text{ m}$$

Environmental disturbances are computed in correspondence of the reference **orbit** reported in Tab. 2.

Table 2: *Initial orbital elements*

a	e	i	Ω	ω	θ_0
6928 km	0.1	53°	30°	15°	0°

2 Requirements

Several element of the develop of the project are imposed in order to study the attitude dynamics and the control system of the spacecraft:

- **attitude determination**: cosine matrices
- **attitude sensors**: Star sensor
- **actuators**: 3 magnetic coils

However the in the following parameters it will be show that the sensors and the actuators mentioned above are not sufficient in order to compute the attitude determination and control.
pointing requirements:
An ipotetical mission was carried out considering a nadir pointing. therefore the attitude control is developed considering the following requirements:

- $A_{\mathrm{B/L}} = I_3$
- $\omega = \begin{bmatrix} 0 & 0 & n^{(1)} \end{bmatrix}^{\mathsf{T}}$

3 ADCS Architecture

In this section the technical specifications of the selected ADCS components will be provided.

3.1 Attituude sensors

3.1.1 Gyroscope - STIM202 (*Sensonor, AS*)

Table 3: *Gyro datasheet*

ARW	RRW	Sampling rate	Power	Mass	Dimensions
0.2 deg/h$^{0.5}$	0.3 deg/h	1000 Hz	5.5 W	55 g	$(39 \times 45 \times 20)$ mm

3.1.2 Earth Horizon Sensor - MAI-SES (*Maryland Aerospace, Inc.*)

Table 4: *EH datasheet*

Configuration	Accuracy	FoV	Voltage	Current (per sensor)	Mass	Dimensions
4 thermopile detectors	$< 0.25°$	7°	3.3 V	40 mA	33 g	$(43.3 \times 31.7 \times 31.7)$ mm

3.1.3 Star Tracker - STANDARD NST-GEN2 (*Blue Canyon Technologies, Inc.*)

Table 5: *ST datasheet*

Accuracy	FoV	Voltage	Power	Mass	Dimensions
$<$ 6 arcsec	10°	5 V	1.5 W	360 g	$(100 \times 55 \times 50)$ mm

3.1.4 Magnetometer - MM200 (*Hyperion Technologies, B.V.*)

Table 6: *MM datasheet*

Accuracy	range	Power	Mass	Dimensions
$< 1.18\ nT/\sqrt{Hz}$	$\pm 800 \mu T$	1∇•5 mA	10 g	$(20 \times 20 \times 11.3)$ mm

[1] n spacecraft mean motion

3.2 Actuators

3.2.1 Magnetorquers - NCTR-M012 (*NewSpace Systems, Ltd.*)

Table 7: *MH datasheet*

Magnetic dipole Sampling rate	Residual induction	Power	Mass	Dimensions
1.19 Am^2 <500 Hz	< 0.005 Am^2	<800 mW	50 g	$(94 \times 15 \times 13)$ mm

In order to achieve three-axis control, 3 orthogonal torque rods are employed.

3.2.2 Reaction Wheels - RW400 (*Hyperion Technologies, B.V.*)

Table 8: *RW datasheet*

Maximum torque	Total momentum storage	Power	Mass	Dimensions
8 mNm	15 mNms	1000 mW	155 g	$(50 \times 50 \times 27)$ mm

In order to achieve three-axis control, 3 orthogonal RW are employed.

4 Spacecraft Dynamics and Kinematics

4.1 Orbital Mechanics

In order to obtain the the position vector, the velocity vector and the keplerian parameter during the orbital period, the restricted two body problem equation is integrated, in this model the effects of perturbations are neglected.

$$\frac{\mathrm{d}^2\underline{\mathbf{r}}}{\mathrm{d}t^2} = -\frac{\mu}{r^3}\underline{\mathbf{r}} \tag{1}$$

The position vector and the velocity vector obtained by integration allows to compute all the keplerian parameters, than it is possible to compute the LVLH matrix.

$$A_{\mathrm{L/N}} = R_3(\omega + \theta)R_1(i)R_3(\Omega) \tag{2}$$

All of these parameters are computed in the Simulink block called *"Orbit_propagator"* that is shown in figure 16.

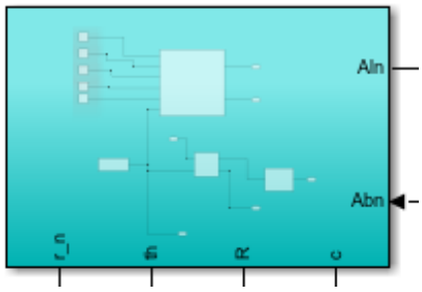

Figure 2: *Orbit_propagator*

4.2 Attitude Dynamics

The attitude of the cubesat is computed considering the spacecraft as a rigid body by integrating Euler's Eqs.

$$J\dot{\underline{\boldsymbol{\omega}}} = J\underline{\boldsymbol{\omega}} \times \underline{\boldsymbol{\omega}} + \underline{\mathbf{u}} + \underline{\mathbf{d}} \tag{3}$$

which, using principal coordinates, can be rewritten as:

$$\begin{cases} \dot{\omega}_{\mathrm{x}} = \dfrac{J_{\mathrm{y}} - J_{\mathrm{z}}}{J_{\mathrm{x}}}\omega_{\mathrm{y}}\omega_{\mathrm{z}} + \dfrac{u_{\mathrm{x}} + d_{\mathrm{x}}}{J_{\mathrm{x}}} \\ \dot{\omega}_{\mathrm{y}} = \dfrac{J_{\mathrm{z}} - J_{\mathrm{x}}}{J_{\mathrm{y}}}\omega_{\mathrm{x}}\omega_{\mathrm{z}} + \dfrac{u_{\mathrm{y}} + d_{\mathrm{y}}}{J_{\mathrm{y}}} \\ \dot{\omega}_{\mathrm{z}} = \dfrac{J_{\mathrm{x}} - J_{\mathrm{y}}}{J_{\mathrm{z}}}\omega_{\mathrm{x}}\omega_{\mathrm{y}} + \dfrac{u_{\mathrm{z}} + d_{\mathrm{z}}}{J_{\mathrm{z}}} \end{cases}$$

All of these parameters are computed in the Simulink block called *"DYNAMICS"* that is shown in figure 16.

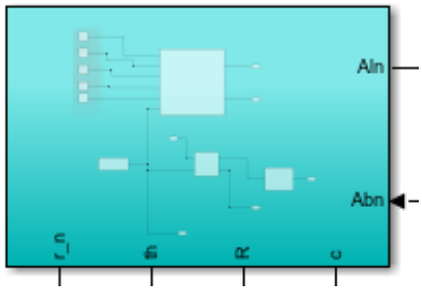

Figure 3: *Orbit_propagator*

4.3 Attitude Kinematics

the attitude matrix of the spacecraft is computed in the subsystem called *"KINEMATICS"* shown in figure 16.

4.3.1 DCM representation

As mentioned in 2 one of the project constraint consist in the developing of the attitude kinematics using the direction cosine matrices.
the time derivatives of the attitude matrices is computed using the equation 4.

$$\frac{\mathrm{d}A}{\mathrm{d}t} = -[\underline{\boldsymbol{\omega}}\wedge]A(t) \tag{4}$$

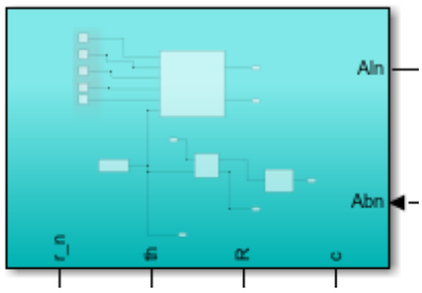

Figure 4: *Orbit_propagator*

where: $[\underline{\boldsymbol{\omega}}\wedge] = \begin{bmatrix} 0 & -\omega_3 & \omega_2 \\ \omega_3 & 0 & -\omega_1 \\ -\omega_2 & \omega_1 & 0 \end{bmatrix}$

Then, knowing $\underline{\boldsymbol{\omega}}$ by dynamics subsystem it is possible to integrate the equation 4 in order to update the matrix A.
Since the integration is done numerically, the orthogonality is lost after some steps. It is necessary to orthogonalize the matrix A after some steps, an approximate solution can be evaluated with this recursive formula:

$$A_{k+1}(t) = \frac{3}{2}A_k(t) - \frac{1}{2}A_k(t)A_k(t)^{\intercal}A_k(t) \tag{5}$$

4.3.2 comparison with quaternion representation

The comparison is based on the attitude matrix by using the quaternion representation, the results are shown in figure 16. the orthonormal condition can be checked by analyzing the determinant of the attitude matrix that can be visualized in (inserisci ref e figure).

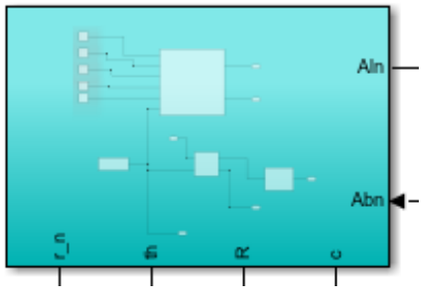

Figure 5: *Orbit_propagator*

5 Environmental Disturbances

In this report a low earth orbit with low eccentricity is analyzed. In this region the main disturbance torques take into account are the following:

- **Gravity Gradient torque**
- **Solar Radiation Pressure**
- **Magnetic torque**
- **Air Drag Atmospheric torque**

All the disturbance torques are computed in the simulink subsystem *"DISTURBANCES"* shown in figure 16.

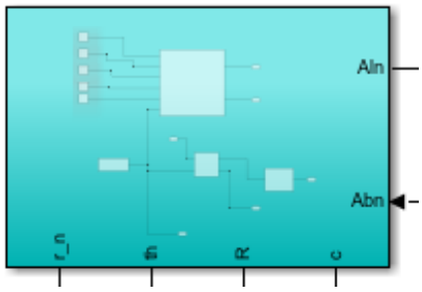

Figure 6: *Orbit_propagator*

5.1 Gravity Gradient torque

As a result of the non-uniformity of the gravity field over the S/C's body, a non-negligible torque will arise. Even if the torque is small the effect can be considerable due the long time action.
the GGT is computed by integration of the elementary force due to gravity acting along the S/C mass, then in order to evaluate the effect on the satellite dynamics, has to be evaluated in the principal axis frame. this procedure yeld:

$$\underline{\mathbf{M}}_{\mathrm{GG}} = \frac{3Gm_{\mathrm{earth}}}{r^3} \cdot \begin{Bmatrix} \dfrac{J_{\mathrm{z}} - J_{\mathrm{y}}}{J_{\mathrm{x}}} c_3 c_2 \\ \dfrac{J_{\mathrm{x}} - J_{\mathrm{z}}}{J_{\mathrm{y}}} c_1 c_3 \\ \dfrac{J_{\mathrm{y}} - J_{\mathrm{x}}}{J_{\mathrm{z}}} c_2 c_1 \end{Bmatrix} \tag{6}$$

$$\text{where } \begin{Bmatrix} c_1 \\ c_2 \\ c_3 \end{Bmatrix} := A_{\mathrm{B/L}} \begin{Bmatrix} 1 \\ 0 \\ 0 \end{Bmatrix}$$

5.2 Solar Radiation Pressure

The solar radiation illuminating the spacecraft surface generate pressure, that in turn generates a force and a torque around the center of mass of the satellite.The electromagnetic radiation level is basically given by three main contributions:

- direct solar radiation ($\sim 1358\ \frac{\mathrm{W}}{\mathrm{m}^2}$, practically constant at all altitudes)
- solar radiation reflected by Earth
- earth's own radiation

The last two contributions are instead strongly dependent on the altitude. In correspondence of the analyzed orbit it is possible to consider $F_{\mathrm{e}} = 1358 + 580 + 143.4 = 2081.4\ \frac{\mathrm{W}}{\mathrm{m}^2} \rightarrow P = \frac{F_{\mathrm{e}}}{c} = 6.938\ \mu\mathrm{Pa}$.
The model strategy consist in a decomposition of the satellite external structure into a set of flat surfaces, each of which is associated with given specular and diffuse reflection coefficients (ρ_{s} and ρ_{d}). Then, from the knowledge of the relative Sun direction in the body frame $\hat{\underline{\mathbf{s}}} = A_{\mathrm{B/N}} \hat{\underline{\mathbf{S}}}^{\mathrm{N}}$, one may compute:

$$\underline{\mathbf{M}}_{\mathrm{SRP}} = \sum_{\mathrm{i}} \left((\underline{\mathbf{r}}_{\mathrm{CP_i}} - \underline{\mathbf{r}}_{\mathrm{CG_i}}) \times \underline{\mathbf{F}}_{\mathrm{i}} \right)$$

where

$$\underline{\mathbf{F}}_{\mathrm{i}} = \begin{cases} -PA_{\mathrm{i}}(\hat{\underline{\mathbf{n}}}_{\mathrm{i}} \cdot \hat{\underline{\mathbf{s}}}) \left[(1-\rho_{\mathrm{s}})\hat{\underline{\mathbf{s}}} + \left(2\rho_{\mathrm{s}}(\hat{\underline{\mathbf{n}}}_{\mathrm{i}} \cdot \hat{\underline{\mathbf{s}}}) + \frac{2}{3}\rho_{\mathrm{d}} \right) \hat{\underline{\mathbf{n}}}_{\mathrm{i}} \right] & \text{if } \hat{\underline{\mathbf{n}}}_{\mathrm{i}} \cdot \hat{\underline{\mathbf{s}}} > 0 \\ \underline{\mathbf{0}} & \text{if } \hat{\underline{\mathbf{n}}}_{\mathrm{i}} \cdot \hat{\underline{\mathbf{s}}} \leq 0 \end{cases} \tag{7}$$

5.3 Magnetic torque

5.3.1 Magnetic Field Model

In a low earth orbit the effect of Magnetic torque is important, moreover as mentioned in 2 in this project three magnetic coils are used. For these reason an accurate model of the earth magnetic field is requested.
In this report is presented a spherical harmonic expansion model based on the paper *"Mathematical Modeling of Earth's Magnetic Field"* **inserisci bib**. Whit this model the magnetic field is computed in spherical coordinates as the gradient of a scalar potential, $\underline{\mathbf{B}} = -\nabla V$ where V is the potential function. the complete theory can be found in the **inserisci bib** while in this section are represented the most important equations.

$$V(r,\theta,\phi) = a \sum_{\mathrm{n}=1}^{k} \left(\frac{a}{r} \right)^{n+1} \sum_{\mathrm{m}=0}^{n} (g_{\mathrm{n}}^{m} \cos m\phi + h_{\mathrm{n}}^{m} \sin m\phi) P_{\mathrm{n}}^{m}(\theta) \tag{8}$$

$$\begin{cases} B_{\mathrm{r}} = -\frac{\partial V}{\partial r} = \sum_{\mathrm{n}=1}^{k} \left(\frac{a}{r} \right)^{n+2} (n+1) \sum_{\mathrm{m}=0}^{n} (g_{\mathrm{n}}^{m} \cos m\phi + h_{\mathrm{n}}^{m} \sin m\phi) P_{\mathrm{n}}^{m}(\theta) \\ B_{\theta} = -\frac{1}{r}\frac{\partial V}{\partial \theta} = -\sum_{\mathrm{n}=1}^{k} \left(\frac{a}{r} \right)^{n+2} \sum_{\mathrm{m}=0}^{n} (g_{\mathrm{n}}^{m} \cos m\phi + h_{\mathrm{n}}^{m} \sin m\phi) \frac{\partial P_{\mathrm{n}}^{m}(\theta)}{\partial \theta} \\ B_{\phi} = -\frac{1}{r \sin\theta}\frac{\partial V}{\partial \phi} = -\frac{1}{\sin\theta} \sum_{\mathrm{n}=1}^{k} \left(\frac{a}{r} \right)^{n+2} \sum_{\mathrm{m}=0}^{n} m(-g_{\mathrm{n}}^{m} \sin m\phi + h_{\mathrm{n}}^{m} \cos m\phi) P_{\mathrm{n}}^{m}(\theta) \end{cases} \tag{9}$$

where: g_{n}^{m} and h_{n}^{m} are called Gaussian coefficient and are avalible in tabular form up to order 13.
the magnetic field obtained has to be rotated in cartesian coordinate, this operation is computed by means of the right ascension $\alpha(t)$ and the declination $\delta(t)$.

5.3.2 Magnetic torque computation

In order to compute the disturbance torque the magnetic field has to be rotated in principal axis by using the attitude matrix:

$$\underline{\mathbf{B}}_{\mathrm{B}} = A_{\mathrm{B/N}} \underline{\mathbf{B}}_{\mathrm{N}} \tag{10}$$

The magnetic disturbance torque is caused by the interaction between Earth's magnetic field, as given by Eq. 10, and the residual magnetic induction due to on-board currents through wirings/electronics. Such parasitic induction is difficult to model, which makes it typical to consider a worst-case scenario in which we assume $\underline{\mathbf{m}} = \begin{bmatrix} 0.1 & 0.1 & 0.1 \end{bmatrix}^{\intercal}$ Am^2.

The corresponding disturbance torque is hence computed as:

$$\underline{\mathbf{M}}_{\mathrm{magn}} = \underline{\mathbf{m}} \times \underline{\mathbf{B}}_{\mathrm{B}} \tag{11}$$

5.4 Air Drag Atmospheric torque

The underlying idea of our modeling strategy is the same one mentioned in section 5.2 that of decomposing the S/C's external structure into a set of flat surfaces (defined by normal unit vectors $\underline{\hat{\mathbf{n}}}_{\mathrm{i}}$) and then compute the overall torque caused by drag as the superposition of each individual contribution:

$$\begin{aligned}\underline{\mathbf{d}}_{\mathrm{drag}} &= \sum_{\mathrm{i}} \underline{\mathbf{r}}_{\mathrm{i}} \times \underline{\mathbf{F}}_{\mathrm{i}} \\ &= \sum_{\mathrm{i}} \left((\underline{\mathbf{r}}_{\mathrm{CP_i}} - \underline{\mathbf{r}}_{\mathrm{CG_i}}) \times \underline{\mathbf{F}}_{\mathrm{i}} \right)\end{aligned}$$

where

$$\begin{aligned}\underline{\mathbf{v}}_{\mathrm{r}}^{\mathrm{N}} &= \underline{\mathbf{v}}_{\mathrm{ECI}} + \underline{\boldsymbol{\omega}}_{\mathrm{earth}} \times \underline{\mathbf{r}}_{\mathrm{ECI}} \\ \underline{\mathbf{v}}_{\mathrm{r}} &= A_{\mathrm{B/N}} \underline{\mathbf{v}}_{\mathrm{r}}^{\mathrm{N}}\end{aligned}$$

$$\underline{\mathbf{F}}_{\mathrm{i}} = \begin{cases} -\frac{1}{2} C_{\mathrm{D}} \rho v_{\mathrm{r}}^2 (\underline{\hat{\mathbf{n}}}_{\mathrm{i}} \cdot \underline{\hat{\mathbf{v}}}_{\mathrm{r}}) A_{\mathrm{i}} \underline{\hat{\mathbf{v}}}_{\mathrm{r}} & \text{if } \underline{\hat{\mathbf{n}}}_{\mathrm{i}} \cdot \underline{\hat{\mathbf{v}}}_{\mathrm{r}} > 0 \\ \underline{\mathbf{0}} & \text{if } \underline{\hat{\mathbf{n}}}_{\mathrm{i}} \cdot \underline{\hat{\mathbf{v}}}_{\mathrm{r}} \leq 0 \end{cases} \tag{12}$$

A constant value of $\rho = 1.454 \cdot 10^{-13} \frac{kg}{m^3}$ was assumed for the density, according to the model provided in [**vallado2001fundamentals**]. For the drag coefficient a worst-case scenario approach was instead adopted, setting it to $C_{\mathrm{D}} = 2.2$.[(2)]

5.5 Overall value of disturbance torques

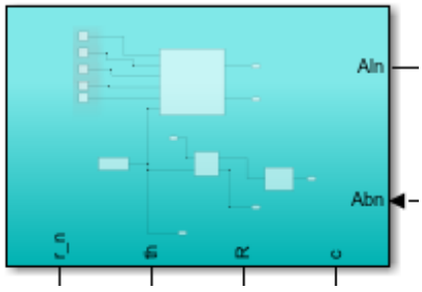

Figure 7: *Orbit_propagator*

inserisci valore massimo dei disturbi

6 Attitude Determination

In this section the determination of the attitude behaviour of the satellite during his own orbit is presented. The sensors are modelled in order to obtain the measure of the attitude matrix and $A_{\mathrm{B/Nest}}$ and the angular velocity ω_{est} in principal axis frame.

these computation are developed in the simulink subsystem *"attitude determination"* shown in figure 16.

[(2)] C_{D} values of a satellite typically ranging between 1.6 and 2.2

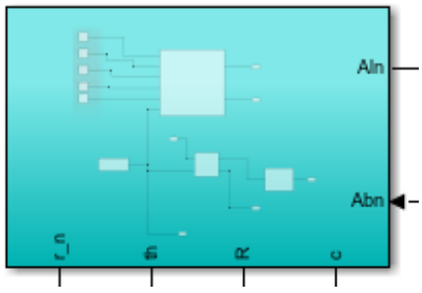

Figure 8: *Orbit_propagator*

6.1 Attitude sensor modelling

The attitude sensor used during the simulation are the ones introduced in 3.

6.1.1 Gyroscope

The raw measurement coming from the gyroscope will be inevitably affected by the presence of noise, which results in the presence of both a noise term and a bias term in the angular velocity output:

$$\underline{\boldsymbol{\omega}}_{\text{meas}} = \underline{\boldsymbol{\omega}} + \underline{\mathbf{n}} + \underline{\mathbf{b}} \tag{13}$$

- ARW: $\underline{\mathbf{n}} = \sigma_{\text{n}} \underline{\boldsymbol{\xi}}_{\text{n}}$ $\longleftarrow$ due to thermo-mechanical noise
- RRW: $\dot{\underline{\mathbf{b}}} = \sigma_{\text{b}} \underline{\boldsymbol{\xi}}_{\text{b}}$ $\longleftarrow$ due to electronic noise (*flicker*)

Both ARW and RRW have been modeled as a Gaussian noise,[(3)] according to the specifications provided in Tab. 3.

6.1.2 Star sensor, Earth horizon sensor and Magnetometer

The reading of such sensors is thus simply modeled as the "true" values[(4)], superimposed with a random noise whose amplitude is determined by the sensor accuracy reported in Tabs. 5, 4. The model follow the one developed during the labs and do not take in account the limitation due to the sensor FOV. Another simplification consist into consider the same accuracy for the roll, pitch and yaw angles. this yelds to:

$$\underline{\mathbf{s}}_{\text{B}} = A_{\varepsilon_{\text{SS}}} A_{\text{B/N}} \underline{\mathbf{s}}_{\text{N}} \tag{14}$$

$$\underline{\mathbf{r}}_{\text{B}} = A_{\varepsilon_{\text{EH}}} A_{\text{B/N}} \underline{\mathbf{r}}_{\text{N}} \tag{15}$$

$$\underline{\mathbf{B}}_{\text{B}} = A_{\varepsilon_{\text{MM}}} A_{\text{B/N}} \underline{\mathbf{B}}_{\text{N}} \tag{16}$$

Where: $A_\varepsilon = \begin{bmatrix} \cos\psi\cos\theta & \cos\psi\sin\theta\sin\phi + \sin\psi\cos\phi & -\cos\psi\sin\theta\cos\phi + \sin\psi\sin\phi \\ -\sin\psi\cos\theta & -\sin\psi\sin\theta\sin\phi + \cos\psi\cos\phi & \sin\psi\sin\theta\cos\phi + \cos\psi\sin\phi \\ \sin\theta & -\cos\theta\sin\phi & \cos\theta\cos\phi \end{bmatrix}$

6.2 Attitude Determination Algorithm

We will make use of the **SVD** method, which has been developed within the framework of Wabha's problem. The latter consists in minimizing the weighted cost function

$$\mathcal{J} = \frac{1}{2} \sum_{\text{i}=1}^{N} \alpha_{\text{i}} \left\| \underline{\hat{\mathbf{v}}}_{\text{B}_{\text{i}}} - A_{\text{B/N}} \underline{\hat{\mathbf{v}}}_{\text{N}_{\text{i}}} \right\|$$

(3) i.e. having zero mean and $\text{std}(f) = \sigma(f)$

(4) i.e. determined by the propagation of the orbit and the cubesat attitude

in which N sensor measurements $\hat{\underline{\mathbf{v}}}_{\mathrm{B_i}}$ are available,[5] along with the corresponding estimations $A_{\mathrm{B/N}}\hat{\underline{\mathbf{v}}}_{\mathrm{N_i}}$ computed using on-board models; in addition the weighting coefficients α_{i} are chosen based on the accuracy of each sensor. The algorithm makes use of the following procedure:

$$\begin{aligned} B &:= \sum_{\mathrm{i}=1}^{N} \alpha_{\mathrm{i}} \hat{\underline{\mathbf{v}}}_{\mathrm{B_i}} \hat{\underline{\mathbf{v}}}_{\mathrm{N_i}}^{\mathsf{T}} \\ B &\overset{\mathrm{SVD}}{=} U\,S\,V^{\mathsf{T}} \\ M &= \begin{bmatrix} 1 & 0 & 0 \\ 0 & 1 & 0 \\ 0 & 0 & \det\{U\}\cdot\det\{V\} \end{bmatrix} \\ A_{\mathrm{B/N}} &= U\,M\,V^{\mathsf{T}} \end{aligned} \tag{17}$$

6.3 Noise Filtering

Both the gyro output and the raw estimated attitude will be inevitably affected by the presence of noise. Making use of a frequency-based LPF would be unsuitable for real time processing. Indeed, filtering the original signal would result in an excessive phase delay, which in turn translates into a delayed control law. Thus, it has been chosen to employ a **state observer**, that basically acts as a filter but with no delay. For instance, in the event of gyro-noise filtering:

$$J\dot{\hat{\underline{\boldsymbol{\omega}}}} = J\hat{\underline{\boldsymbol{\omega}}} \times \hat{\underline{\boldsymbol{\omega}}} + \underline{\mathbf{u}} + \underline{\mathbf{d}} + \alpha(\hat{\underline{\boldsymbol{\omega}}} - \underline{\boldsymbol{\omega}}_{\mathrm{raw}}) \tag{18}$$

where $\alpha < 0$ is a tuning parameter.
An analogous procedure is carried out for filtering the raw attitude estimation.

6.4 Attitude Determination Results

The results obtained with the previous procedure are shown in the figure 16.

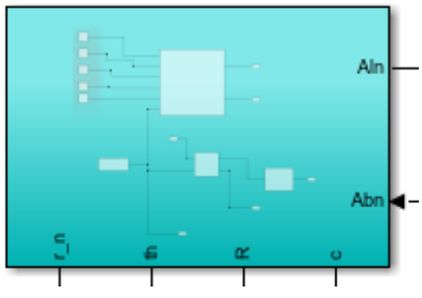

Figure 9: *Orbit_propagator*

7 Attitude Control System

In this section the control system with the control logic and the actuators is analyzed the correspondent Simulink subsystem is shown in figure 16.

[5] $\hat{\underline{\mathbf{v}}}$ denotes the direction of an inertial reference, e.g. the Sun, Earth's center, a star, etc.

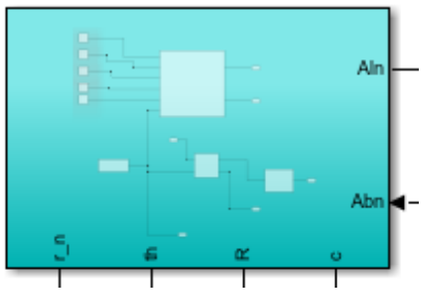

Figure 10: *Orbit_propagator*

7.1 Control Laws

In this project two types of control logic are used:

- **B_dot feedback algorithm**
- **Lyapounov control function**

7.1.1 B_dot Feedback Algorithm

This control law represent a good option to an initial de-tumbling phase in which the main objective is to slow down the spacecraft.

In order to obtain this kind of control action a magnetometer, three magnetic coils and one gyroscope are needed. The control action is based on the following relation:

$$\underline{\mathbf{U}_{\mathrm{c}}} = \underline{\mathbf{m}} \times \underline{\mathbf{B}} \tag{19}$$

$$\underline{\mathbf{m}} = -m_{\max} \cdot \operatorname{sgn}(\underline{\dot{\mathbf{B}}}) \tag{20}$$

Where $\underline{\dot{\mathbf{B}}}$ can be approximated as follow:

$$\underline{\dot{\mathbf{B}}} \approx \underline{\mathbf{B}} \times \underline{\boldsymbol{\omega}} \tag{21}$$

7.1.2 Lyapounov Control Function

in order to achieve the earth pointing requirements let's consider the problem of tracking a generic time-varying desired attitude A_{d} as well as maintaining a desired angular velocity $\underline{\boldsymbol{\omega}}_{\mathrm{d}}$.

A suitable Lyapounov cost function based on DCM is:

$$V = \frac{1}{2}\underline{\boldsymbol{\omega}}_{\mathrm{e}}^{\mathsf{T}} J \underline{\boldsymbol{\omega}}_{\mathrm{e}} + 2K_2 \mathrm{tr}(I - A_{\mathrm{e}}) \tag{22}$$

That leads to a DCM control law[(6)]:

$$\underline{\mathbf{U}}_{\mathrm{id}} = -k_1 \underline{\boldsymbol{\omega}}_{\mathrm{e}} - k_2 \left[A_{\mathrm{e}}^{\mathsf{T}} - A_{\mathrm{e}}\right]^{\vee} + \underline{\boldsymbol{\omega}} \times J\underline{\boldsymbol{\omega}} + J(A_{\mathrm{e}}\underline{\dot{\boldsymbol{\omega}}}_{\mathrm{d}} - \underline{\boldsymbol{\omega}}_{\mathrm{e}} \times A_{\mathrm{e}}\underline{\boldsymbol{\omega}}_{\mathrm{d}}) \tag{23}$$

where: $A_{\mathrm{e}} = AA_{\mathrm{d}}^{\mathsf{T}}$, $\underline{\boldsymbol{\omega}}_{\mathrm{e}} = \underline{\boldsymbol{\omega}} - A_{\mathrm{e}}\underline{\boldsymbol{\omega}}_{\mathrm{d}}$ are respectively the attitude and the angular velocity error, while $A_{\mathrm{d}} = A_{\mathrm{L/N}}$ and $\omega = \begin{bmatrix} 0 & 0 & n \end{bmatrix}^{\mathsf{T}}$ as mentioned in 2.

[(6)] $[\ ]^{\vee}$ denotes the inverse-hat operator, i.e. it maps a skew-symmetric matrix back to its generating vector

7.2 Actuators

7.2.1 Control with 3 magnetic coils

The first control phase which consist in a reduction of the satellite angular velocity is achieved using a set of three orthogonal magnetic coils. The control law is the one described in section 7.1.1 and the maximum magnetic dipole $m_{\max}$ allowed is the one described in **??**.

This kind of control action does not enable to reach a perfect pointing, this is due to the fact that is not possible to generate three independent measure of magnetic control action, therefore in this project this control law is used for the first $300sec$ in order to decrease the control action needed for the following phases.

7.2.2 Control with 2 magnetic coils and 1 RW

As mentioned in section 7.2.1 using three orthogonal magnetic coils it is never possible to generate three independent measure of control torque.

In order to avoid this problem a configuration with two magnetic coils respectively along the x,y direction and one reaction wheel on the z direction is adopted. This configuration allowed to use the control law described in section **??**. The modeling of the actuators follow the one described during the class lectures and can be splitted in three stage:

- Compute the two magnetic dipole and the reaction wheel effort

$$\begin{Bmatrix} m_x \\ m_y \\ -\dot{h}_z \end{Bmatrix} = \frac{1}{B_z} \begin{bmatrix} 0 & -1 & 0 \\ 1 & 0 & 0 \\ B_x & B_y & B_z \end{bmatrix} \begin{Bmatrix} M_x \\ M_y \\ M_z \end{Bmatrix} \tag{24}$$

- apply the actuator limit described in tab **??** and in tab. 8.

- rebuild the real control torque applied by the actuators using the inverse relation of equation 24:

$$\begin{Bmatrix} M_x \\ M_y \\ M_z \end{Bmatrix} = \begin{bmatrix} 0 & B_z & 0 \\ -B_z & 0 & 0 \\ B_y & -B_x & 1 \end{bmatrix} \begin{Bmatrix} m_x \\ m_y \\ -\dot{h}_z \end{Bmatrix} \tag{25}$$

in the following figure the required ideal control torque and the ones generated by the actuators are represented. 16.

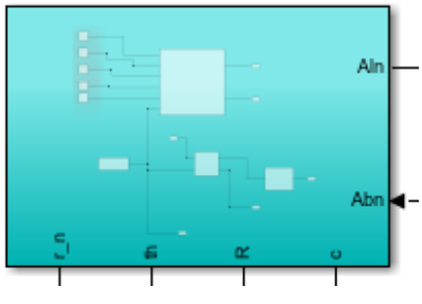

Figure 11: *Orbit_propagator*

in the fig. 16 it is possible to see that the real control action is much lower with respect to the one required by the control law.

A deeper analysis provide that the limiting factor are the magnetic coils[7]. In spite of this limited control torque the pointing requirement can be reached:

[7] during the second stage an important factor is that it is not sufficient cut the exceeding required magnetic dipole to the maximum available. The torque generated by the actuators has to be proportional to the one provided by the control law, this leads to a reduction of all the torque components.

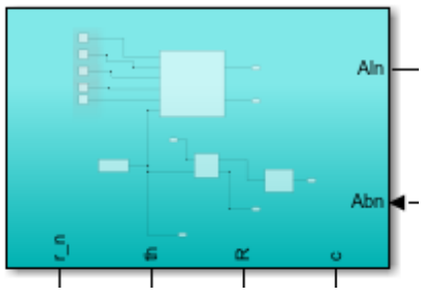

Figure 12: *Orbit_propagator*

The figure 16 show that a good pointing is reached after **inserisci tempo** that is much higher than one orbital period.

7.2.3 Control with 3 RW

Even this control action is commanded by the control law described in section 7.1.2. This time different from the previous section the control action is provided by three orthogonal RW disposed along the three principal axis. As described before the modeling of the actuators follow the one described during the class lectures and can be subdivided in three steps:

- Compute the reaction wheels effort

$$\dot{\underline{\mathbf{h}}}_{\mathrm{r}} = -A^{*}(\underline{\mathbf{M}}_{\mathrm{c}} + \underline{\boldsymbol{\omega}} \times A\underline{\mathbf{h}}_{\mathrm{r}})^{(8)} \tag{26}$$

- apply the actuator limit described in tab. 8.
- rebuild the real control torque applied by the actuators using the inverse relation of equation 24:

$$\underline{\mathbf{U}}_{\mathrm{c}} = -(\underline{\boldsymbol{\omega}} \times A\underline{\mathbf{h}}_{\mathrm{r}} + A\dot{\underline{\mathbf{h}}}_{\mathrm{r}}) \tag{27}$$

where A is the configuration matrix that in this particular case simply leads to $A = I_3$.

The next figure show the comparison between the ideal control action and the one gives by the RW.

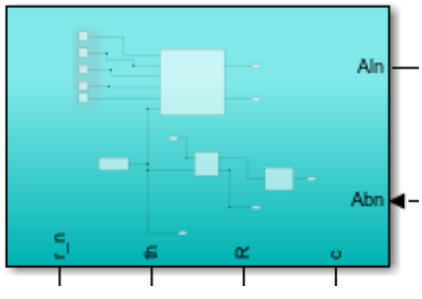

Figure 13: *Orbit_propagator*

Give a look at fig. 16 and **inserisci riferimenti** can be noticed as the last control is more similar to the ideal one with respect to the previous one. Even in this case the pointing requirement can be satisfied:

(8) the symbol * denotes the pseudo-inverse matrix

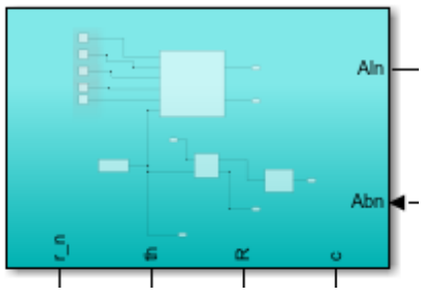

Figure 14: *Orbit_propagator*

In this case as it is possible to see in figure **inserisci ref** the pointing is successfully reached in a lower time with respect to what is shown in section 7.2.2.

the problem with this kind of control action resides inside the saturation limit of the reactions wheels. This kind of actuator has a limit on the total storable torque as described in tab. 8. So that after some time it is maybe possible that the reaction wheels can not more provide the torque necessary in order to control the spacecraft attitude.

7.3 Final Configuration Pointing Results

In order to avoid the issues cited in section 7.2.2 and 7.2.3 a multistep phase configuration is adopted:

1. **Phase 1: three magnetic coils detumbling** This phase is the one mentioned above in section 7.2.1. in this phase an initial slow down of the spacecraft is provided by the three orthogonal magnetic coils by using the control law described in section 7.1.1.

2. **Phase 2: three reaction wheels pointing** In this phase the actuators control logic described in section 7.2.3 is used for $50sec$ in order complete the pointing reaching without exceed the reaction wheels saturation limit.

3. **Phase 3: pointing maintenance with 2 magnetic coils and one RW** Once the pointing has been reached the actuators logic described in section 7.2.2 allows to maintain the earth pointing requirement because the control torque needed is not too high as in phase 2.

   This solution is a good option also from the RW saturation view point, in fact once the reaction wheels reach the maximum storable torques, it is sufficient to turn off the reaction wheel and switch on the magnetic coil of the corresponding axis and make the inverse procedure on one of the another two axis[(9)].

In the following figures the final simulation results in terms of attitude matrix and angular velocity along one orbital period are provided.

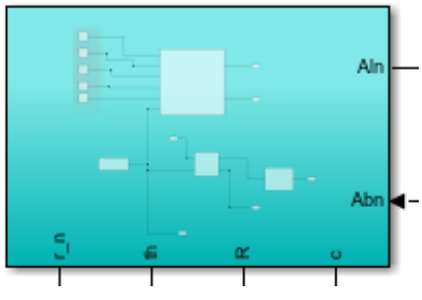

Figure 15: *Orbit_propagator*

[(9)]This procedure requires also a little correction on the computation of the control torque described in section 7.2.2

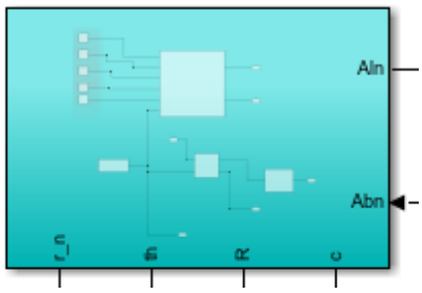

Figure 16: *Orbit_propagator*

8 Conclusion

In this report the develop of a spacecraft attitude control simulation is presented. through Simulink, a good model of the satellite orbit, dynamic, kinematic, environmental disturbances and attitude determination and control system are implemented.

The simulation leads to the attitude control choice and the results presented in **??**, However some observation has to be done.

This report is presented with an academic purpose, both in the attitude sensors and in the actuators an high redundancy is evidenced. This is good for a safety view point but results to much expensive form a energy budget and a cost budget.

From the attitude determination point of view two sensors are sufficient for a complete determination. In this sense the magnetometer is necessary to be used because provide also the measure of the magnetic field necessary to compute the control action in the first and in the third phases, while during an hypothetical real mission the EH sensor can be use only when the star sensor has not the possibility to provide any measurement or when an higher precision on attitude estimation is necessary.

A similar analysis can be carried out for the actuators set. If the real mission do not have any time constraint from a pointing view point, in section 7.2.2 it is shown that the pointing requirement can be achieved also with only one reaction wheels instead of the three requested in the final choice, also the desaturation of the wheel can be done in this case alternating the control action for the pointing with the one used during the phase 1.

Nevertheless this solution that savings cost it is very poor from a safety view point, in fact the failure of the reaction wheel do not allow with the procedure of the mission. Even the performance are poor, during the desaturation phases a good pointing can not be achievable for the reason given in section 21. These two points can be solved easily adding one RW, however the maximum torque allowed with the configuration mentioned above remains too low to reject unforseen disturbances like a small impact.

for this reason although the configuration with only one RW seems feasible, in this report it was preferred to present a more conservative solution.